Stochastic Geometry Analysis for RIS-Assisted Large-Scale Cellular Networks

Tianxiong Wang*, Gaojie Chen†, Mihai-Alin Badiu*, and Justin P. Coon*
*Department of Engineering Science, University of Oxford, Oxford, OX1 3PJ, United Kingdom
†5GIC & 6GIC, Institute for Communication Systems (ICS), University of Surrey, Guildford, GU2 7XH, United Kingdom
e-mail: {tianxiong.wang, justin.coon, mihai.badiu}@eng.ox.ac.uk, gaojie.chen@surrey.ac.uk

***Abstract*—In this paper, we analyze the coverage probability of a reconfigurable intelligent surface (RIS) aided cellular network with the theory of stochastic geometry. A Poisson cluster process (PCP) is applied to model the positions of transmitters (TXs) and RISs, capturing their spatial correlations. Considering the general Nakagami-m fading channel model, we derive the approximate distributions of the composite channel gains with RIS-assisted transmission, representing the desired signal channel and the interference channel, respectively. The coverage probability of the typical user is then obtained. The derived coverage probability is in a closed form, which can be evaluated efficiently. Simulation results are presented to show that the presented analysis is effective, demonstrate the significant performance gains brought by the passive beamforming of a RIS with a large number of elements, and show the impact of TX density on the performance of the proposed system.**

***Index Terms*—Reconfigurable intelligent surface, performance analysis, stochastic geometry**

I. Introduction

Using reconfigurable intelligent surfaces (RISs) to improve the quality of wireless communications has been viewed as a promising physical layer (PHY) technology in wireless communication networks [1]. A RIS comprises massive low-cost and passive reflecting elements, which can perform passive beamforming of the incident waves, focusing the reflected waves towards the receiver [2]. Owing to the prominent advantages of RISs in providing cost-effective, energy-efficient, and reliable wireless communications, the implementations of RISs have been widely explored in recent years, e.g., RIS aided non-orthogonal multiple access (NOMA) [3], physical layer security [4], unmanned aerial vehicle (UAV) communications [5], [6].

As a brand new technology, numerous research efforts in the academic field have been devoted to characterizing the performance of RIS-aided wireless networks. Up to the present, most existing works focus on the single-cell system and conduct link-level performance analysis. The authors in [7] used the central limit theorem (CLT) to obtain the outage probability of a RIS-aided communication link with perfect phase shifting. With a similar system setup, the authors in [8] investigated the asymptotic behavior of the outage probability in the large transmit signal-to-noise ratio (SNR) regime and derived the diversity order. Moreover, the authors in [9] took phase errors into consideration and proved that the composite channel gain with phase errors follows the Nakagami-m distribution. The authors in [10] illustrated that the CLT-based approaches are only valid when the number of reflecting elements is very large and in the low SNR regime. Therefore, a moment matching technique based on the gamma distribution was proposed, which can give an accurate approximation even with a small number of elements. Then, the performance of a RIS-assisted communication link with perfect and random phase adjustment over Nakagami-m fading channels were investigated in [11] and [12], respectively. The Nakagami-m channel model is regarded as a more general option than Rayleigh.

Even though the link-level analysis attracts more research interests, the system-level analysis considering multiple transmitters (TXs), users and RISs was also carried out in a few works. The blockages and RISs were jointly modeled by the boolean line segments in [13], where the authors investigated the connection probability that each user can be served by a RIS, and showed the benefits of implementing RISs in service coverage extension. The authors in [14] used two independent homogeneous Poisson point processes (HPPP) to model the positions of TXs and RISs, respectively. The signal power and interference power distributions and the coverage probability were derived. The authors in [15] analyzed the coverage probability and ergodic rate of a RIS empowered large-scale NOMA system where the locations of TXs and users followed two independent HPPP. Considering the users served and not served by RISs, the authors in [16] analyzed the network coverage probability and investigated the impact of the proportions of different types of users on the system performance.

It is worth noting that all the existing works regarding the RIS-assisted multi-cell networks do not take the spatial correlations between the positions of TXs and RISs into consideration. However, to provide more reliable transmission, the locations of the assisting RISs should be designed carefully according to the locations of TXs; therefore, the positions of TXs and RISs are spatially correlated in practice. To this end, we jointly model the locations of TXs and RISs as a Poisson cluster process (PCP), and analyze the coverage probability of the typical user. The general Nakagami-m fading channel model is applied, and both the direct links and the RIS reflected channels are considered. Particularly, the distributions of the signal power and the interference power are derived, and the coverage probability of the typical user

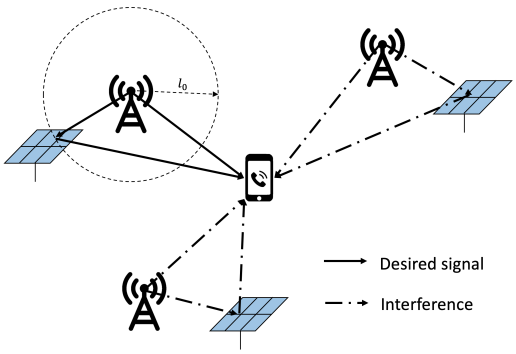

Fig. 1. System model of the RIS-assisted large-scale cellular networks.

is given in a closed form. Numerical results are presented to illustrate the performance gains brought by the passive beamforming of RIS and demonstrate the impact of the density of TXs on the network performance.

II. System Model

The system model studied in this paper is a RIS-aided large-scale wireless network, including multiple TXs, users, and RISs. All the TXs and users are equipped with a single antenna, and we focus on the downlink transmission from the TXs to users. The system model is shown in Fig. 1. It is assumed that the locations of users follow a HPPP. On the other hand, the locations of TXs and RISs are jointly assumed to be a PCP with two nodes in each cluster. To be specific, the locations of TXs are modeled by a HPPP Φ_t with the density of λ_t, which is the parent process. For each TX in Φ_t, a daughter node, standing for the assisting RIS, is uniformly distributed in a circle with the radius of l_0, centered at the location of the corresponding TX[1]. The daughter process of the locations of RISs is denoted as Φ_r. In this paper, we analyze the performance of the typical user, denoted as U_0.

A. Channel Model

It is assumed that each RIS has M elements. We denote the normalized small scale fading of the channels from a TX to its corresponding RIS and from a RIS to U_0, i.e., T_i-$R_{i'}$, $i \in \Phi_t$, $i' \in \Phi_r$, and $R_{i'}$-U_0 respectively as $\mathbf{g}_i$ and $\mathbf{r}_i$, such that

$$\mathbf{g}_i = (g_{i,1}, ..., g_{i,M})^T \in \mathbb{C}^{M\times 1}, \tag{1a}$$

$$\mathbf{r}_i = (r_{i,1}, ..., r_{i,M})^T \in \mathbb{C}^{M\times 1}. \tag{1b}$$

In this paper, we assume all the channels associated with the RISs are Nakagami-m fading with unit power, such that

$$|g_{i,m}| \sim \text{Nakagami}(n_g, 1) \tag{2a}$$

$$|r_{i,m}| \sim \text{Nakagami}(n_r, 1), \tag{2b}$$

where $m \in \{1, 2, ..., M\}$; n_g and n_r denote the Nakagami-m shape parameters of $|g_{i,m}|$ and $|r_{i,m}|$, respectively. The large scale fading of the T_i-$R_{i'}$-U_0 channel is given by

$$\alpha_{r,i} = \beta_r (l_0 d_{r,i})^{-\nu}, \tag{3}$$

where β_r is the large scale fading per unit distance of the reflected channel; l_0 and $d_{r,i}$ are the distances of the T_i-$R_{i'}$ channel and the $R_{i'}$-U_0 channel, respectively; ν denote the pathloss exponent.

The direct link from a TX to U_0, i.e., T_i-U_0, $i \in \Phi_t$, is assumed to be a Rayleigh fading channel, and the channel gain can be given as

$$h_i = \sqrt{\alpha_{h,i}}\,\xi_i = \sqrt{\beta_h d_{h,i}^{-\nu}}\,\xi_i, \tag{4}$$

where β_h is the large scale fading per unit distance of the T_i-U_0 channel; $d_{h,i}$ is the distance between T_i and U_0; ξ_i is a normalized complex Gaussian random variable such that $\xi_{h,i} \sim \mathcal{CN}(0, 1)$.

B. Signal Model

The signal received at the typical user U_0 can be written as

$$y = \left(\sqrt{\alpha_{r,0}}\mathbf{g}_0^T \mathbf{\Theta}_0 \mathbf{r}_0 + \sqrt{\alpha_{h,0}}\xi_0\right)\sqrt{P}x_0 + \sqrt{P}\hat{I} + w_0, \tag{5}$$

where

$$\hat{I} = \sum_{k\in\Phi_t\backslash\{0\}} \left(\sqrt{\alpha_{r,k}}\mathbf{g}_k^T \mathbf{\Theta}_k \mathbf{r}_k + \sqrt{\alpha_{h,k}}\xi_k\right) x_k \tag{6}$$

denotes the interference power; P is the transmit power of each TX; x_k is the transmit constellation symbol with zero mean and unit variance; $\mathbf{\Theta}_k = \text{diag}\left(e^{j\theta_{k,1}}, ..., e^{j\theta_{k,M}}\right)$ represents the phase adjustment matrix of $R_{k'}$. w_0 is the additive white Gaussian noise (AWGN), i.e., $w_0 \sim \mathcal{CN}(0, \sigma_0^2)$.

To maximize the received SNR of U_0, the phases of R_0 are shifted to align the phases of the RIS channels to the direct link, such that[2]

$$\theta_{0,m} = -\arg(g_{0,m}) - \arg(r_{0,m}) + \arg(\xi_0). \tag{7}$$

Furthermore, the phases of the interference channels, i.e., T_k-$R_{k'}$-U_0, $k \in \Phi_t\backslash\{0\}$, are uniformly distributed over $[0, 2\pi)$. Hence, the signal received by U_0 is rewritten as

$$y = \left(\sqrt{\alpha_{r,0}}\sum_{m=1}^{M}|g_{0,m}||r_{0,m}| + \sqrt{\alpha_{h,0}}|\xi_0|\right)e^{j\arg(\xi_0)}\sqrt{P}x_0 + \sqrt{P}\hat{I} + w_0, \tag{8}$$

where

$$\hat{I} = \sum_{k\in\Phi_t\backslash\{0\}} \hat{I}_k, \tag{9a}$$

$$\hat{I}_k = \left(\sqrt{\alpha_{r,k}}\sum_{m=1}^{M}|g_{k,m}||r_{k,m}|e^{j\phi_{k,m}} + \sqrt{\alpha_{h,k}}\xi_k\right)x_k, \tag{9b}$$

[1]For clarity, we investigate the case where the distance between a TX and its corresponding RIS is fixed. The presented results can be generalized to other patterns of the PCP model by averaging over the distribution of l_0, which will constitute our future work.

[2]We consider the continuous phase shifting without phase errors, which leads to a performance upper bound [17]. Moreover, the performance of 2-bit phase adjustment is close to the ideal case [18].

and $\phi_{k,m}$ follows the uniform distribution within $[0, 2\pi)$. Thus, the received SNR can be written as

$$\gamma = \frac{S}{I + \gamma_t^{-1}}, \tag{10}$$

where

$$S = \left(\sqrt{\alpha_{r,0}} \sum_{m=1}^{M} |g_{0,m}||r_{0,m}| + \sqrt{\alpha_{h,0}}|\xi_0| \right)^2, \tag{11a}$$

$$I = \sum_{k \in \Phi_t \backslash \{0\}} I_k = \sum_{k \in \Phi_t \backslash \{0\}} |\hat{I}_k|^2, \tag{11b}$$

and γ_t is the transmit SNR such that $\gamma_t = P/\sigma_0^2$.

III. Signal and Interference Power Analysis

In this section, the distributions of the desired signal power S and the interference power I are analyzed in detail.

A. Signal Power Analysis

The desired signal power S can be written as

$$S = \left(\sqrt{\alpha_{r,0}} S_1 + \sqrt{\alpha_{h,0}}|\xi_0| \right)^2, \tag{12}$$

where

$$S_1 = \sum_{m=1}^{M} |g_{0,m}||r_{0,m}|. \tag{13}$$

The distribution of S_1 is evaluated first. Here, a moment matching approach is proposed to approximate the distribution of S_1. The moment matching method aims to match the mean and second-order raw moment of a random variable of which the exact distribution is intractable for analysis to another random variable with known distribution. Given that $|g_{0,m}|$ and $|r_{0,m}|$, $m \in \{1, ..., M\}$ follow the Nakagami-m distribution and they are independent and identically distributed (i.i.d.) random variables, we can derive the mean and second-order raw moment of S_1 as:

$$\begin{aligned} \mathbb{E}[S_1] &= \sum_{m=1}^{M} \mathbb{E}[|g_{0,m}|] \mathbb{E}[|r_{0,m}|] \\ &= M (n_g n_r)^{-\frac{1}{2}} \frac{\Gamma\left(n_g + \frac{1}{2}\right)}{\Gamma(n_g)} \frac{\Gamma\left(n_r + \frac{1}{2}\right)}{\Gamma(n_r)}, \end{aligned} \tag{14}$$

$$\begin{aligned} \mathbb{E}\left[S_1^2\right] &= \mathbb{E}\left[\sum_{m=1}^{M} |g_{0,m}|^2 |r_{0,m}|^2 \right] \\ &\quad + 2\,\mathbb{E}\left[\sum_{m=1}^{M-1} \sum_{i=m+1}^{M} |g_{0,m}|\,|r_{0,m}|\,|g_{0,i}|\,|r_{0,i}| \right] \\ &= M + \frac{M(M-1)}{n_g n_r} \left(\frac{\Gamma\left(n_g + \frac{1}{2}\right)}{\Gamma(n_g)} \frac{\Gamma\left(n_r + \frac{1}{2}\right)}{\Gamma(n_r)} \right)^2, \end{aligned} \tag{15}$$

where $\Gamma(\cdot)$ is the gamma function. Thus, we can fit S_1 as the gamma distribution, of which the shape and scale parameters are

$$\kappa_1 = \frac{\mathbb{E}^2[S_1]}{\mathbb{E}[S_1^2] - \mathbb{E}^2[S_1]}, \quad \omega_1 = \frac{\mathbb{E}[S_1^2] - \mathbb{E}^2[S_1]}{\mathbb{E}[S_1]}. \tag{16}$$

Based on the approximate distribution of S_1, the mean and second-order raw moment of S can be derived as

$$\mathbb{E}[S] = \alpha_{h,0}\eta_1, \tag{17a}$$

$$\mathbb{E}\left[S^2\right] = \alpha_{h,0}^2 \eta_2, \tag{17b}$$

where

$$\alpha = \sqrt{\alpha_{r,0}/\alpha_{h,0}}, \tag{18a}$$

$$\eta_1 = \vartheta_2^h + 2\alpha\vartheta_1^h\vartheta_1^\tau + \alpha^2\vartheta_2^\tau, \tag{18b}$$

$$\eta_2 = \vartheta_4^h + 4\alpha\vartheta_3^h\vartheta_1^\tau + 6\alpha^2\vartheta_2^h\vartheta_2^\tau + 4\alpha^3\vartheta_1^h\vartheta_3^\tau + \alpha^4\vartheta_4^\tau. \tag{18c}$$

ϑ_b^ϵ, $\epsilon \in \{h, \tau\}$ is the bth order raw moment of $|\xi_0|$ and S_1, respectively. Since $|\xi_0|$ is a Rayleigh variable with the parameter $\sqrt{2}/2$, i.e., $|\xi_0| \sim \mathcal{R}(\sqrt{2}/2)$, and S_1 is approximated by a gamma random variable, ϑ_b^h and ϑ_b^τ are given by

$$\vartheta_b^h = \Gamma\left(1 + \frac{1}{2}b\right), \tag{19a}$$

$$\vartheta_b^\tau = \omega_1^b \frac{\Gamma(b + \kappa_1)}{\Gamma(\kappa_1)}. \tag{19b}$$

Hence, we can fit S as the gamma distribution, of which the shape and scale parameters are

$$\kappa = \frac{\eta_1^2}{\eta_2 - \eta_1^2}, \tag{20a}$$

$$\omega = \alpha_{h,0}\bar{\eta} = \alpha_{h,0}\frac{\eta_2 - \eta_1^2}{\eta_1}. \tag{20b}$$

The cumulative distribution function (CDF) and probability density function (PDF) of S can be given as

$$F_S(x) = \frac{\gamma(\kappa, x/\omega)}{\Gamma(\kappa)}, \tag{21a}$$

$$f_S(x) = \frac{x^{\kappa-1} \exp(-x/\omega)}{\Gamma(\kappa)\,\omega^\kappa}, \tag{21b}$$

where $\gamma(\cdot, \cdot)$ is the lower incomplete gamma function.

B. Interference Power Analysis

The interference power from T_k, $k \in \Phi_t \backslash \{0\}$ can be written as

$$I_k = \left| \sqrt{\alpha_{r,k}} I_{1,k} + \sqrt{\alpha_{h,k}} \xi_k \right|^2, \tag{22}$$

where

$$I_{1,k} = \sum_{m=1}^{M} |g_{k,m}||r_{k,m}| e^{j\phi_{k,m}}. \tag{23}$$

Since $\phi_{k,m}$ follows the uniform distribution within $[0, 2\pi)$, the central limit theorem (CLT) can be applied directly to fit $I_{1,k}$ as a circularly symmetric complex Gaussian (CSCG) random variable for a large number of RIS elements, such that

$$I_{1,k} \sim \mathcal{CN}(0, M). \tag{24}$$

Moreover, since ξ_k is also a CSCG random variable, we can have

$$\sqrt{\alpha_{r,k}} I_{1,k} + \sqrt{\alpha_{h,k}} \xi_k \sim \mathcal{CN}(0, M\alpha_{r,k} + \alpha_{h,k}). \tag{25}$$

Therefore, we can learn that I_k is an exponentially distributed random variable, of which the PDF and CDF can be given as

$$f_{I_k}(x) = \frac{1}{M\alpha_{r,k} + \alpha_{h,k}} \exp\left(-\frac{x}{M\alpha_{r,k} + \alpha_{h,k}}\right), \quad (26a)$$

$$F_{I_k}(x) = 1 - \exp\left(-\frac{x}{M\alpha_{r,k} + \alpha_{h,k}}\right). \quad (26b)$$

In contrast to the moment matching approach in the signal power distribution analysis, the approach based on the CLT method is applied in the interference power analysis. The reasons are explained as follows. First, in the signal power analysis, S_1 is a positive random variable. Thus, fitting S_1 with a gamma variable makes more sense since the gamma distribution is always positive. However, a Gaussian random variable is supported in the set of reals. Therefore, applying the CLT to fit S_1 causes significant errors. The authors in [10] also introduced this point. Different from S_1, the supports of the real and imaginary parts of $I_{1,k}$ are both the set of reals. Hence, it is more reasonable to use the CLT to fit the distribution of $I_{1,k}$ as CSCG distribution.

Remark 1. *By using the CLT, the distribution of I_k is not related to the Nakagami-m distribution parameters.*

C. Laplace Transform of the Interference Power

The Laplace transform of the interference power is proposed in the following proposition, which will be used when we characterize the coverage probability.

Proposition 1. *If U_0 is connected with a TX at a fixed location*[3]*, the Laplace transform of the interference power can be given as*

$$\mathcal{L}_I(s) = \exp\left(-\frac{2\pi^2\lambda_t \csc\left(\frac{2\pi}{\nu}\right)}{\nu}\left((M\beta_r l_0^{-\nu} + \beta_h)s\right)^{\frac{2}{\nu}}\right), \quad (27)$$

Proof: See the Appendix. □

IV. Coverage Probability Analysis

In this section, we characterize the coverage probability of U_0. The coverage probability is an important performance metric that can be used to evaluate the reliability of a communication network. It is defined as the probability that the received SINR is larger than a threshold, i.e.,

$$P_c(\gamma_0) = \mathbb{P}(\gamma > \gamma_0). \quad (28)$$

Using the approximate signal power distribution and the Laplace transform of the interference power, the coverage probability of the typical user can be evaluated and concluded in the following proposition.

[3]In this paper, we consider the fixed connection strategy. Discussion on the nearest connection strategy will be left for the future work.

Proposition 2. *If U_0 is connected with a TX at a fixed location, the coverage probability of U_0 is*

$$P_c(\gamma_0) = \sum_{j=0}^{\bar{\kappa}-1} \frac{(-1)^j}{j!}\left[\frac{\partial^j}{\partial s^j} X(s)\right]_{s=1}, \quad (29)$$

where

$$X(s) = \exp\left(-\frac{\gamma_0\gamma_t^{-1}}{\omega}s\right)\mathcal{L}_I\left(\frac{\gamma_0}{\omega}s\right), \quad (30)$$

and $\bar{\kappa}$ is the integer closest to κ; $\mathcal{L}_I(s)$ is defined in (27)*.*

Proof: The desired signal power distribution has been fitted by the gamma distribution with the scale parameter κ. Another approximation is taken here by rounding κ to the closest integer $\bar{\kappa}$. Then, the coverage probability of U_0 can be written as

$$\begin{aligned} P_c(\gamma_0) &= \mathbb{P}(\gamma > \gamma_0) \\ &= \mathbb{E}_I\left[\bar{F}_S(\gamma_0(I + \gamma_t^{-1}))\right] \\ &= \mathbb{E}_Y\left[\frac{\Gamma(\bar{\kappa}, Y)}{\Gamma(\bar{\kappa})}\right], \end{aligned} \quad (31)$$

where

$$Y = \left(I + \gamma_t^{-1}\right)\frac{\gamma_0}{\omega}, \quad (32)$$

and $\Gamma(\cdot,\cdot)$ is the upper incomplete gamma function, which can be expanded in series. Then, we can have

$$\begin{aligned} P_c(\gamma_0) &= \sum_{j=0}^{\bar{\kappa}-1}\frac{(-1)^j}{j!}\mathbb{E}_Y\left[(-1)^j Y^j e^{-Y}\right] \\ &= \sum_{j=0}^{\bar{\kappa}-1}\frac{(-1)^j}{j!}\mathbb{E}_Y\left[\left[\frac{\partial^j}{\partial s^j}e^{-sY}\right]_{s=1}\right] \\ &\overset{(a)}{=} \sum_{j=0}^{\bar{\kappa}-1}\frac{(-1)^j}{j!}\left[\frac{\partial^j}{\partial s^j}\mathbb{E}_Y\left[e^{-sY}\right]\right]_{s=1} \\ &= \sum_{j=0}^{\bar{\kappa}-1}\frac{(-1)^j}{j!}\left[\frac{\partial^j}{\partial s^j}\mathcal{L}_Y(s)\right]_{s=1}, \end{aligned} \quad (33)$$

where (a) follows by using the interchangeable properties of computing differentiation and expectation.

Using the derived Laplace transform of the interference power in Proposition 1, the Laplace transform of Y is written by

$$\begin{aligned} \mathcal{L}_Y(s) &= \mathbb{E}_I\left[\exp\left(-(I + \gamma_t^{-1})\frac{\gamma_0}{\omega}s\right)\right] \\ &= \exp\left(-\frac{\gamma_0\gamma_t^{-1}}{\omega}s\right)\mathcal{L}_I\left(\frac{\gamma_0}{\omega}s\right). \end{aligned} \quad (34)$$

Thus, the proof is complete. □

Remark 2. *Regarding the Proposition 2, it can be learned that increasing the density of TXs λ_t and reducing the transmit SNR γ_t will lead to lower coverage probability due to the increased interference power and the decreased signal power, respectively.*

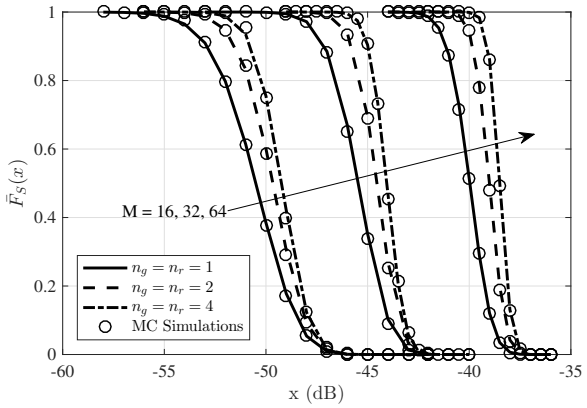

Fig. 2. CCDF of S and MC simulation results.

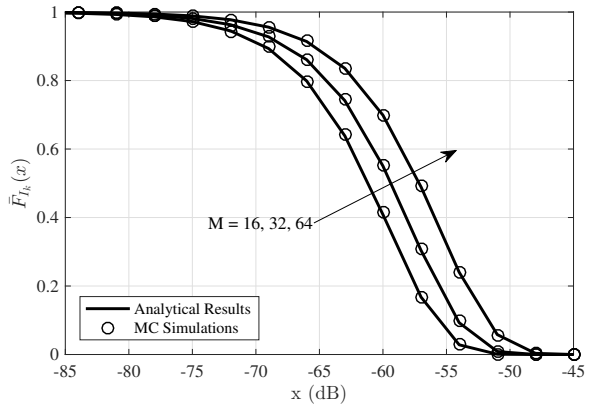

Fig. 3. CCDF of I_k and MC simulation results.

V. Numerical Results

If not otherwise specified, the Monte Carlo (MC) simulation parameters are provided in the following. We generate all the nodes of the PCP in a circle area, of which the radius is $5000\,\mathrm{m}$. The large scale fading per unit distance and the pathloss exponent are set as $\beta_h = \beta_r = -30\,\mathrm{dB}$ and $\nu = 2.5$, respectively. The distribution radius of the daughter node of the PCP is $l_0 = 3\,\mathrm{m}$. Since the fixed connection strategy is investigated in this paper, U_0 is at the origin, while the TX and the RIS connected with U_0 are respectively located at the coordinates of $(20, 0)$ and $(20, 3)$. The noise power σ_0^2 is set to be $-70\,\mathrm{dBm}$. The SINR threshold $\gamma_0 = 0\,\mathrm{dB}$.

Fig. 2 is presented to demonstrate the accuracy of fitting S as the gamma distribution. It can be learned that the proposed analytical results match with the MC simulations very well. Moreover, we can see that the received signal power can be greatly increased by adding the number of RIS elements due to the passive beamforming. According to the simulation results, $n_g = n_r = 1$ and the CCDF of S, $\bar{F}_S(x) = 0.8$, it can be observed that $x = -41\,\mathrm{dB}$ and $x = -52\,\mathrm{dB}$ for $M = 64$ and $M = 16$, respectively.

On the other hand, Fig. 3 illustrates the accuracy of fitting I_k as an exponential random variable. To demonstrate the advantage of RIS passive beamforming, we place the interfering TX and RIS at the coordinates of $(0, 20)$ and $(3, 20)$, respectively. The approximation based on the CLT also has high accuracy in terms of fitting the interference power. Compared with the results in Fig. 2, the interference power is much weaker due to the lack of passive beamforming. It is worth noting that the interference power does not increase as quickly as the signal power when the number of RIS elements increases, showing that using a large RIS is beneficial for the communication quality in a multi-cell network.

Fig. 4 shows the coverage probability versus the transmit SNR with different densities of TXs. Simulation parameters are set as $l_0 = 3\,\mathrm{m}$, $n_g = n_r = 2$. The elements equipped at each RIS is $M = 32$. It can be learned that increasing the density of TXs will deteriorate the performance of the typical user due to the increased interference power level.

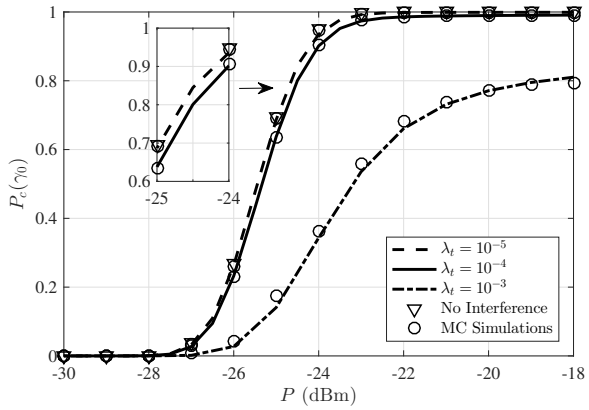

Fig. 4. Coverage probability against transmit power.

However, when the density of TXs is smaller than $10^{-4}\,/\mathrm{m}^2$, the performance of U_0 is very close to the 'No Interference' case, where there are not any interfering TXs. Hence, in a network with sparsely deployed TXs, the link-level analysis carried out in many existing works can well represent the network performance.

VI. Conclusions

This paper presented a RIS-assisted cellular network with multiple TXs, RISs, and users. The typical user is connected with a fixed TX with an assisting RIS, while all the interfering TXs and RISs follow a PCP, capturing the spatial correlations. The distributions of the signal power and the interference power, as well as the coverage probability of the typical user are analyzed in detail. It was shown that, with passive beamforming, increasing the number of RIS elements can significantly improve the network performance. In the proposed system setup with the fixed connection strategy, a larger density of TXs will lead to worse performance due to the increased interference.

$$\mathcal{L}_I(s) \overset{(b)}{=} \exp\left(2\pi\lambda_t \int_0^\infty \left(\frac{1}{1+s(M\beta_r l_0^{-\nu}+\beta_h)r^{-\nu}}-1\right) r\,\mathrm{d}r\right)$$
$$= \exp\left(-\frac{2\pi^2\lambda_t \csc\left(\frac{2\pi}{\nu}\right)}{\nu}\left((M\beta_r l_0^{-\nu}+\beta_h)s\right)^{\frac{2}{\nu}}\right). \tag{35}$$

APPENDIX

With the fixed connection strategy, the Laplace transform of the interference power can be written as

$$\begin{aligned}\mathcal{L}_I(s) &= \mathbb{E}\left[e^{-sI}\right] \\ &= \mathbb{E}\left[\exp\left(-s\sum_{k\in\Phi_t\setminus\{0\}} I_k\right)\right] \\ &= \mathbb{E}\left[\prod_{k\in\Phi_t\setminus\{0\}} \exp\left(-sI_k\right)\right] \\ &\overset{(a)}{=} \mathbb{E}\left[\prod_{k\in\Phi_t\setminus\{0\}} \frac{1}{1+\left(N\alpha_{r,k}+\alpha_{h,k}\right)s}\right],\end{aligned} \tag{36}$$

where (a) follows that I_k is exponentially distributed. Analytically, $d_{r,k}$, l_0 and $d_{h,k}$ follow the law of cosines, such that

$$d_{r,k} = \sqrt{d_{h,k}^2 + l_0^2 - 2d_{h,k}l_0\cos\left(\varpi_{r,k}\right)}, \tag{37}$$

where $\varpi_{r,k}$ is the angle contained between the T_k-U_0 link and the T_k-$R_{k'}$ link, which is random variable uniformly distributed over $[0, 2\pi)$. However, since the spatial correlation is considered between TXs and RISs, we can safely assume that $d_{h,k} \gg l_0$ if the RIS is deployed in the vicinity of its corresponding TX for the exchange of channel state information (CSI). Moreover, as introduced in many papers, RIS might be used to serve cell-edge users which are far away from the TX in the future, and TXs are deployed sparsely in practical networks, where $10^{-3}/\mathrm{m}^2$ is a large value. These practical insights make the assumption more reasonable. In this way, we are able to take a distance approximation that $d_{h,k} \approx d_{r,k}$. Hence, the Laplace transform of the interference power can be derived as in (35), where (b) follows from the probability generating functional (PGFL).

ACKNOWLEDGMENTS

This research was funded in part by EPSRC grant number EP/T02612X/1. For the purpose of Open Access, the author has applied a CC BY public copyright licence to any Author Accepted Manuscript (AAM) version arising from this submission.

REFERENCES

[1] S. Dang, O. Amin *et al.*, "What should 6G be?" *Nat. Electron.*, vol. 3, no. 1, pp. 20–29, 2020.

[2] Q. Wu and R. Zhang, "Towards smart and reconfigurable environment: Intelligent reflecting surface aided wireless network," *IEEE Commun. Mag.*, vol. 58, no. 1, pp. 106–112, 2020.

[3] T. Wang, M.-A. Badiu *et al.*, "Outage probability analysis of STAR-RIS assisted NOMA network with correlated channels," *IEEE Commun. Lett.*, 2022, Early Access.

[4] C. Huang, G. Chen, and K.-K. Wong, "Multi-agent reinforcement learning-based buffer-aided relay selection in IRS-assisted secure cooperative networks," *IEEE Trans. Inf. Forensics Security*, vol. 16, pp. 4101–4112, 2021.

[5] L. Yang, F. Meng *et al.*, "On the performance of RIS-assisted dual-hop UAV communication systems," *IEEE Trans. Veh. Technol.*, vol. 69, no. 9, pp. 10 385–10 390, 2020.

[6] T. Wang, M.-A. Badiu *et al.*, "Outage probability analysis of RIS-assisted wireless networks with Von Mises phase errors," *IEEE Wireless Commun. Lett.*, vol. 10, no. 12, pp. 2737–2741, 2021.

[7] D. Kudathanthirige, D. Gunasinghe, and G. Amarasuriya, "Performance analysis of intelligent reflective surfaces for wireless communication," in *Proc. IEEE Int. Conf. Commun. (ICC)*, Dublin, Ireland, Jun. 2020, pp. 1–6.

[8] T. Wang, G. Chen *et al.*, "Chernoff bound and saddlepoint approximation for outage probability in IRS-assisted wireless systems," in *Proc. IEEE Global Commun. Conf. Wkshps. (GC Wkshps)*, Madrid, Spain, Dec. 2021, pp. 1–5.

[9] M. Badiu and J. P. Coon, "Communication through a large reflecting surface with phase errors," *IEEE Wireless Commun. Lett.*, vol. 9, no. 2, pp. 184–188, 2020.

[10] S. Atapattu, R. Fan *et al.*, "Reconfigurable intelligent surface assisted two–way communications: Performance analysis and optimization," *IEEE Trans. Wireless Commun.*, vol. 68, no. 10, pp. 6552–6567, 2020.

[11] H. Ibrahim, H. Tabassum, and U. T. Nguyen, "Exact coverage analysis of intelligent reflecting surfaces with Nakagami-m channels," *IEEE Trans. Veh. Technol.*, vol. 70, no. 1, pp. 1072–1076, 2021.

[12] S. A. Tegos, D. Tyrovolas *et al.*, "On the distribution of the sum of double-Nakagami-m random vectors and application in randomly reconfigurable surfaces," *IEEE Trans. Veh. Technol.*, 2022, Early Access.

[13] M. A. Kishk and M.-S. Alouini, "Exploiting randomly located blockages for large-scale deployment of intelligent surfaces," *IEEE J. Sel. Areas Commun.*, vol. 39, no. 4, pp. 1043–1056, 2020.

[14] J. Lyu and R. Zhang, "Hybrid active/passive wireless network aided by intelligent reflecting surface: System modeling and performance analysis," *IEEE Trans. Wireless Commun.*, vol. 20, no. 11, pp. 7196–7212, 2021.

[15] C. Zhang, W. Yi *et al.*, "Reconfigurable intelligent surfaces aided multi-cell NOMA networks: A stochastic geometry model," *IEEE Trans. Commun.*, vol. 70, no. 2, pp. 951–966, 2022.

[16] T. Shafique, H. Tabassum, and E. Hossain, "Stochastic geometry analysis of IRS-assisted downlink cellular networks," *IEEE Trans. Commun.*, vol. 70, no. 2, pp. 1442–1456, 2022.

[17] T. Wang, M.-A. Badiu *et al.*, "Performance analysis of IOS-assisted NOMA system with channel correlation and phase errors," *IEEE Trans. Veh. Technol.*, 2022, Early Access.

[18] T. Wang, G. Chen *et al.*, "Study of intelligent reflective surface assisted communications with one-bit phase adjustments," in *Proc. IEEE Global Commun. Conf. (GLOBECOM)*, Virtual, Dec. 2020, pp. 1–6.